Generation of Frequency-Multiplied and Phase-Coded Signal Using an Optical Polarization Division Multiplexing Modulator

Yamei Zhang, *Student Member, IEEE*, Fangzheng Zhang, and Shilong Pan, *Senior Member, IEEE*

***Abstract*— A novel method to generate frequency-multiplied and phase-coded microwave signals based on a polarization division multiplexing (PDM) dual-arm Mach–Zehnder modulator (DMZM) or a PDM dual-parallel MZM (DPMZM) is proposed. In the proposed scheme, the PDM-DMZM or PDM-DPMZM is employed to produce two orthogonally polarized wavelengths with a wavelength spacing that is two, four, or eight times of the driving frequency. Then the signal is sent into a polarization modulator-based microwave photonic phase coder for phase coding. A theoretical analysis and an experiment are carried out. Phase-coded signals with frequency multiplication factors of two, four and eight are successfully generated. The bandwidth of the system is discussed, and the impact of the polarization extinction ratio is also analyzed.**

***Index Terms*— Frequency multiplication, phase coding, polarization modulation, radio frequency (RF) and microwave signal generation, RF photonics.**

I. Introduction

MICROWAVE phase-coded signal generation has been widely investigated in the past decades for pulse compression in radar systems or for spectral efficiency improvement in communication links [1]. Traditionally, electrical methods are employed to generate the phase-coded signals. However, these systems would suffer from the small operational frequency range and complicated setup. To remedy this, optical methods to generate the phase-coded microwave signals were reported, which yields tremendous benefits like broad operation frequency range, low loss, and electromagnetic interference immunity [2], [3]. Up to now, a large number of optical systems were proposed to generate the phase-coded signals [4]–[23], which can be generally divided into two categories. One utilizes optical spectral shaping together with frequency-to-time mapping (FTTM) technology [9]–[11], and the other is based on external phase modulation followed by optical heterodyning [13]–[23].

The methods in the first category are mainly realized based on an optical wave shaper [10], [11] and a dispersive element. For example, in [10], an optical wave shaper is used to shape the spectrum of an ultrashort optical pulse into a sinusoidal profile. Controlling the voltage of the electrical coding signal applied to the system, the output optical spectrum of the wave shaper is shifted accordingly. With the FTTM operation in a dispersive element, the spectral shape is converted into the time domain. Therefore, a phase-coded signal is obtained. However, the setup of this kind of system is complicated, and the generated signal suffers seriously from large noise, poor spectral purity, fixed center frequency, and fixed coding rate.

The basic idea for the methods in the second category is to introduce different phase modulations to two phase-correlated optical wavelengths [13]–[23], followed by optical heterodyning in a photodetector (PD). One approach is to spatially separate the two wavelengths and introduce only one of them to a phase modulator (PM) [13], [14]. This operation, however, would inevitably introduce considerable phase noise to the generated phase-coded signal. To avoid this problem, one can first generate two orthogonally polarized optical wavelengths, and then employ a polarization modulator (PolM) to implement complementary phase modulations on the two polarization directions. The orthogonally polarized optical wavelengths can be generated based on a polarization beam combiner (PBC) [16], a differential group delay (DGD) element [17], [18], or the stimulated Brillouin scattering (SBS) effect [19]. For the PBC-based system [16], phase-coded signals with arbitrary frequency can be generated, but the stability of the system is poor since the two wavelengths are spatially separated; for the DGD-element-based approach [17], [18], due to the frequency dependence of the DGD-induced polarization rotation, phase-coded signals with only several specific frequencies can be generated, and for the SBS-based method [19], several stages of SBS must be employed to rotate the state of the polarization of one of the wavelengths by 90°, which suffers from high power

Manuscript received September 1, 2015; revised November 23, 2015, August 10, 2016, and August 29, 2016; accepted September 4, 2016. Date of publication November 3, 2016; date of current version February 8, 2017. This work was supported in part by the National Natural Science Foundation of China under Grant 61422108, Grant 61401201, and Grant 61527820, in part by the Funding for Outstanding Doctoral Dissertation in NUAA under Grant BCXJ15-02, in part by the Funding of Jiangsu Innovation Program for Graduate Education under Grant KYLX15_0280, and in part by the Fundamental Research Funds for the Central Universities.

The authors are with the Key Laboratory of Radar Imaging and Microwave Photonics, Ministry of Education, Nanjing University of Aeronautics and Astronautics, Nanjing 210016, China (e-mail: pans@ieee.org).

Color versions of one or more of the figures in this paper are available online at http://ieeexplore.ieee.org.

Digital Object Identifier 10.1109/TMTT.2016.2616878

consumption and a complicated structure. Recently, a single-sideband polarization modulation-based [24], [25] phase-coded signal generator is reported [20], which features large operation bandwidth (10–43 GHz), high stability, and compact structure.

Most of the aforementioned systems based on external phase modulation can generate only a signal with a center frequency that equals to the driving frequency. To realize high-frequency phase-coded signal generation using low-frequency devices, schemes that can perform simultaneously frequency multiplying and phase coding are highly desirable [17], [18], [21]–[23]. In [17], phase-coded signals with doubled frequency were generated by carrier-suppressed double-sideband (CS-DSB) modulation incorporated with a DGD element, and in [18], phase-coded signals with a quadrupled frequency were obtained using a polarization-maintaining fiber Bragg grating (FBG). However, simultaneous frequency multiplying and phase coding can be implemented only at several specific frequencies. To obtain large range tunable phase-coded signals with multiplied frequency, a dual-parallel PolM-based approach is reported [21], which can perform simultaneously phase coding and frequency doubling. Though the generator is frequency independent and has large operation bandwidth, it has a poor stability due to the interferometric structure of the dual-parallel PolM, which is realized using discrete optical components. Recently, we proposed another method that can simultaneously perform phase coding and frequency doubling, which is realized based on cascaded Mach–Zehnder modulator (MZM), PolM, and FBG [22]. The system has a straightforward structure that can avoid interference, and features large operation bandwidth and large tunability. However, there are three modulators cascaded in the system, which seriously increase the complexity of the scheme. In addition, the frequency multiplication factor in [21] and [22] is only two. More recently, a photonic approach for simultaneous frequency quadrupling and phase coding was demonstrated using a dual-parallel MZM (DPMZM) and a Sagnac loop incorporating an FBG [23]. The key problem associated with the system is that the two wavelengths are spatially separated, which would lead to a poor stability in practical applications.

In this paper, a scheme that can realize frequency-multiplied and phase-coded signal generation is proposed and demonstrated based on integrated modulators, i.e., an optical polarization division multiplexing (PDM) dual-arm MZM (DMZM) and a PDM-DPMZM. The frequency multiplication factor can be two, four, and eight. The scheme is comprised of a tunable laser source (TLS), a PDM-DMZM or PDM-DPMZM-based orthogonally polarized CS-DSB generator, and a PolM-based phase coder. A light wave from the TLS is sent to the orthogonally polarized CS-DSB generator, which is composed of the PDM-DMZM or PDM-DPMZM with four radio frequency (RF) input ports and an FBG. By controlling the phases of the RF signals and the dc biases of the PDM-DMZM or PDM-DPMZM, double-sideband modulated signals composed of the optical carrier and two optical sidebands, i.e., ±first-order sidebands, ±second-order sidebands, or ±fourth-order sidebands, are generated. With the FBG to suppress the optical carrier, orthogonally polarized sidebands separated by two, four, or eight times of the driving frequency are obtained, which are then injected into the microwave photonic phase coder. In the microwave photonic phase coder, the orthogonally polarized sidebands experience complementary phase modulations in a PolM. With a polarizer to combine the two sidebands, and a PD to perform square-law detection, phase-coded and frequency-multiplied signals are generated. The frequency multiplication factors can be two, four, and eight, which will be introduced in Section II and be experimentally demonstrated in Section III. As far as we know, there are only very few systems that can generate phase-coded signals with frequency multiplication factors larger than four before. The impact of experimental unideal factors, such as the amplitude imbalance of the RF signals, the RF phase shift, the dc-bias-drift of modulators, and the finite polarization extinction ratio, on the system performance are investigated. The proposed scheme features wideband operation, large frequency tunablity, high stability, and compact configuration, which can be potentially employed in radar systems and terahertz systems.

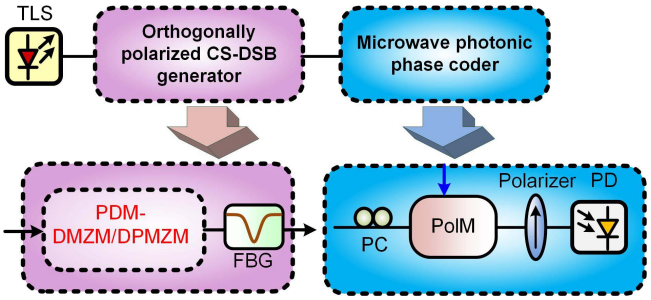

Fig. 1. Schematic of the signal generator that can simultaneously perform phase coding and frequency multiplying.

II. Principle

The setup of the frequency-multiplied and phase-coded signal generator is shown in Fig. 1. The system is comprised of a TLS, an orthogonally polarized CS-DSB generator, and a microwave photonic phase coder. The orthogonally polarized CS-DSB generator that consists of a PDM-DMZM or a PDM-DPMZM and an FBG-based optical filter is employed to generate two orthogonally polarized optical sidebands, i.e., ±first-order sidebands, ±second-order sidebands, or ±fourth-order sidebands. The PolM-based microwave photonic phase coder [20] is used to introduce complementary phase modulations to the two orthogonally polarized sidebands. As a result, electrical phase-coded signals with a center frequency equals to the frequency difference of the two orthogonally polarized sidebands are generated. The frequency multiplication factor can be two, four, and eight.

A. Simultaneous Frequency Doubling and Phase Coding

In order to generate a phase-coded signal with a doubled frequency, an integrated PDM-DMZM is applied in the orthogonally polarized CS-DSB generator. Fig. 2(a) shows the equivalent structure of the PDM-DMZM. The PDM-DMZM is

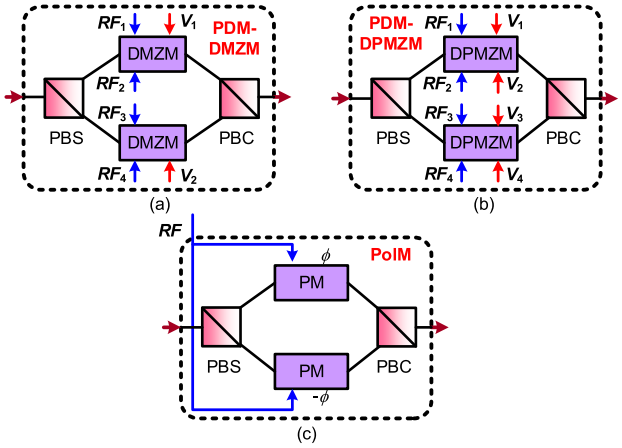

Fig. 2. Schematic of (a) PDM-DMZM, (b) PDM-DPMZM, and (c) PolM.

composed of a polarization beam splitter (PBS), two dual-arm MZMs (each has two RF input ports), and a PBC. Supposing that the expressions of the optical carrier and four electrical driving RF signals are $\exp(j\omega_c t)$, $V_{RF1}\cos(\omega_{RF}t+\phi_1)$, $V_{RF2}\cos(\omega_{RF}t+\phi_2)$, $V_{RF3}\cos(\omega_{RF}t+\phi_3)$, and $V_{RF4}\cos(\omega_{RF}t+\phi_4)$, respectively, where ω_c and ω_{RF} are the angular frequencies of the optical carrier and the RF signals, ϕ_i and V_{RFi} ($i=1$–4) are the phases and peak voltages of the four RF signals, the modulated signal after the PDM-DMZM can be expressed as

$$\begin{cases} E_x = \exp[j\omega_c t + j\beta_1\cos(\omega_{RF}t+\phi_1) + j\varphi_1] \\ \qquad + \exp[j\omega_c t - j\beta_2\cos(\omega_{RF}t+\phi_2)] \\ E_y = \exp[j\omega_c t + j\beta_3\cos(\omega_{RF}t+\phi_3) + j\varphi_2] \\ \qquad + \exp[j\omega_c t - j\beta_4\cos(\omega_{RF}t+\phi_4)] \end{cases} \tag{1}$$

where φ_1 and φ_2 are the phase differences introduced by the dc biases of the two DMZMs, equal to $\pi V_{DCn}/V_\pi$ ($n=1,2$), and β_i equals to $\pi V_{RFi}/V_\pi$, where V_{DCn} and V_π represent the voltage of the dc bias and the half-wave voltage of the PDM-DMZM, respectively. For simplicity, the peak voltages of the four RF signals are assumed to be the same, i.e., $V_{RF1}=V_{RF2}=V_{RF3}=V_{RF4}=V_{RF}$ and $\beta_1=\beta_2=\beta_3=\beta_4=\beta$. Expanding (1) with Bessel functions, the signal becomes

$$\begin{cases} E_x = \exp(j\omega_c t + j\varphi_1)\sum_{m=-\infty}^{\infty} j^m J_m(\beta)\exp[jm(\omega_{RF}t+\phi_1)] \\ \qquad + \exp(j\omega_c t)\sum_{m=-\infty}^{\infty}(-j)^m J_m(\beta)\exp[jm(\omega_{RF}t+\phi_2)] \\ E_y = \exp(j\omega_c t + j\varphi_2)\sum_{m=-\infty}^{\infty} j^m J_m(\beta)\exp[jm(\omega_{RF}t+\phi_3)] \\ \qquad + \exp(j\omega_c t)\sum_{m=-\infty}^{\infty}(-j)^m J_m(\beta)\exp[jm(\omega_{RF}t+\phi_4)] \end{cases} \tag{2}$$

where J_m represents the mth-order Bessel function of the first kind. When $\beta < \pi/6$, the sidebands with orders higher than one can be ignored, so (2) becomes

$$\begin{cases} E_x = \exp(j\omega_c t + j\varphi_1) \\ \qquad \times\left[J_0(\beta) + J_{-1}(\beta)\exp\left(-j\omega_{RF}t - j\phi_1 - j\frac{\pi}{2}\right)\right. \\ \qquad \left. + J_1(\beta)\exp\left(j\omega_{RF}t + j\phi_1 + j\frac{\pi}{2}\right)\right] + \exp(j\omega_c t) \\ \qquad \times\left[J_0(\beta) + J_{-1}(\beta)\exp\left(-j\omega_{RF}t - j\phi_2 + j\frac{\pi}{2}\right)\right. \\ \qquad \left. + J_1(\beta)\exp\left(j\omega_{RF}t + j\phi_2 - j\frac{\pi}{2}\right)\right] \\ E_y = \exp(j\omega_c t + j\varphi_2) \\ \qquad \times\left[J_0(\beta) + J_{-1}(\beta)\exp\left(-j\omega_{RF}t - j\phi_3 - j\frac{\pi}{2}\right)\right. \\ \qquad \left. + J_1(\beta)\exp\left(j\omega_{RF}t + j\phi_3 + j\frac{\pi}{2}\right)\right] + \exp(j\omega_c t) \\ \qquad \times\left[J_0(\beta) + J_{-1}(\beta)\exp\left(-j\omega_{RF}t - j\phi_4 + j\frac{\pi}{2}\right)\right. \\ \qquad \left. + J_1(\beta)\exp\left(j\omega_{RF}t + j\phi_4 - j\frac{\pi}{2}\right)\right]. \end{cases} \tag{3}$$

Letting $\varphi_1=\pi/2$, $\varphi_2=-\pi/2$, $\phi_1=0$, $\phi_2=\pi/2$, $\phi_3=0$, and $\phi_4=\pi/2$ by adjusting the voltages of the dc biases of the PDM-DMZM and the phases of the RF signals, (3) can be simplified as

$$\begin{bmatrix} E_x \\ E_y \end{bmatrix} = \begin{bmatrix} \exp(j\omega_c t)[2J_{-1}(\beta)\exp(-j\omega_{RF}t) + J_0(\beta)(1+j)] \\ \exp(j\omega_c t)[2J_0(\beta)(1-j) + J_1(\beta)\exp(j\omega_{RF}t)] \end{bmatrix}. \tag{4}$$

From (4), we can see that, for both the two polarization directions, optical single-sideband modulations are realized. With the FBG-based optical notch filter to suppress the optical carrier, we obtain

$$\begin{bmatrix} E_x \\ E_y \end{bmatrix} = \begin{bmatrix} \exp(j\omega_c t)[2J_{-1}(\beta)\exp(-j\omega_{RF}t)] \\ \exp(j\omega_c t)[2J_1(\beta)\exp(j\omega_{RF}t)] \end{bmatrix}. \tag{5}$$

From (5), we can see that only the two first-order sidebands are retained, with each sideband along one of the two orthogonal polarization directions. Coupling the two optical wavelengths into a PolM that has an equivalent structure of Fig. 2(c) [26], complementary phase modulations can be introduced to the two orthogonally polarized wavelengths. Supposing that the driving signal to the PolM is $s(t)$, the output of the PolM can be written as

$$\begin{bmatrix} E_x \\ E_y \end{bmatrix} = \begin{bmatrix} 2J_{-1}(\beta)\exp(j\omega_c t - j\omega_{RF}t + j\gamma s(t)) \\ 2J_1(\beta)\exp(j\omega_c t + j\omega_{RF}t - j\gamma s(t)) \end{bmatrix} \tag{6}$$

where γ is the phase modulation index of the PolM. Using a polarizer to combine E_x and E_y, and adjusting the angle between the principal axis of the polarizer and one principal axes of the PolM to be 45°, the signal after the polarizer becomes

$$\begin{aligned} E_{pol} = {} & 2J_{-1}(\beta)\exp(j\omega_c t - j\omega_{RF}t + j\gamma s(t)) \\ & + 2J_1(\beta)\exp(j\omega_c t + j\omega_{RF}t - j\gamma s(t)). \end{aligned} \tag{7}$$

Convert the signal in (7) into an electrical current with a PD, we have

$$I_{AC}(t) \propto J_{-1}(\beta)J_1(\beta)\cos(2\omega_{RF}t - 2\gamma s(t)). \tag{8}$$

From (8), we can see that a frequency-doubled signal with phase associated with γ and $s(t)$ is obtained. When $s(t)$

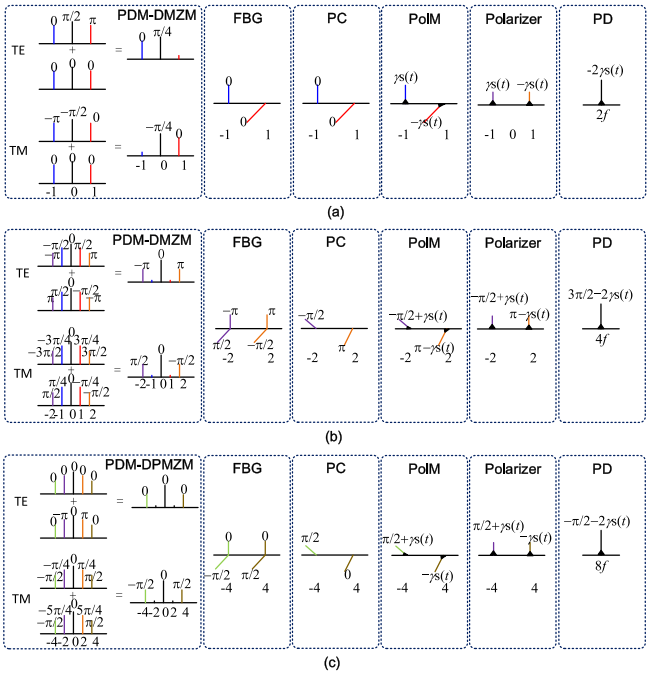

Fig. 3. Schematics of the optical spectra after different devices for (a) frequency-doubling, (b) frequency-quadrupling, and (c) frequency-octupling operation.

is an electrical coding signal, the signal in (8) becomes a phase-coded signal. The phase difference between different bits can be adjusted by the amplitude of $s(t)$. By applying an electrical coding signal with different amplitudes, different phase modulations can be realized. The phase modulation with doubled modulation index is contributed by the complementary phase modulations of the PolM, which can generate the same phase-coded signal with a half amplitude compared with the condition using a single PM. Fig. 3(a) shows the schematics of the optical spectra after different devices for the frequency-doubling operation.

B. Simultaneous Frequency Quadrupling and Phase Coding

By increasing the modulation index β, the ±second-order sidebands in (2) will be too large to be ignored. Then, controlling the dc biases to make $\varphi_1 = \varphi_2 = 0$, and adjusting the phases of the electrical driving RF signals to let $\phi_1 = \phi_2 = 0$ and $\phi_3 = \phi_4 = \pi/4$, the output of the orthogonally polarized CS-DSB generator becomes

$$\begin{cases} E_x = 2\exp(j\omega_c t)[J_{-2}(\beta)\exp(-j2\omega_{RF}t - j\pi) \\ \qquad\qquad +J_2(\beta)\exp(j2\omega_{RF}t + j\pi)] \\ E_y = 2\exp(j\omega_c t)\left[J_{-2}(\beta)\exp\left(-j2\omega_{RF}t + j\dfrac{\pi}{2}\right)\right. \\ \qquad\qquad \left. +J_2(\beta)\exp\left(j2\omega_{RF}t - j\dfrac{\pi}{2}\right)\right]. \end{cases} \tag{9}$$

The signal in (9) is actually a signal having two orthogonally polarized sidebands if a polarization controller (PC) (for instance, the PC in the microwave photonic phase coder) is used to rotate it by θ and add a phase difference of φ_0. The transformation matrix of the PC is

$$T_{PC} = \begin{bmatrix} \cos\theta\exp(j\varphi_0) & -\sin\theta \\ \sin\theta & \cos\theta\exp(-j\varphi_0) \end{bmatrix}. \tag{10}$$

Letting $\theta = \pi/4$ and $\varphi_0 = \pi/2$, we have

$$\begin{bmatrix} E_{x'} \\ E_{y'} \end{bmatrix} = \begin{bmatrix} \exp(j\omega_c t)\left[2J_{-2}(\beta)\exp\left(-j2\omega_{RF}t - j\dfrac{\pi}{2}\right)\right] \\ \exp(j\omega_c t)[2J_2(\beta)\exp(j2\omega_{RF}t + j\pi)] \end{bmatrix}. \tag{11}$$

From (11), we can see that only the –second-order sideband is left for TE mode and the +second-order sideband is left for TM mode. Thereby, an orthogonally polarized CS-DSB modulated signal with ±second-order sidebands is obtained.

Similarly, with a PolM to introduce complementary phase modulations to the two orthogonally polarized ± second-order sidebands, and converting the signal into the electrical domain with a PD, we have

$$I_{AC}(t) \propto J_{-2}(\beta_2)J_2(\beta_2)\cos\left(4\omega_{RF}t + \frac{3\pi}{2} - 2\gamma\, s(t)\right). \tag{12}$$

Therefore, a frequency-quadrupled signal with a phase of $2\gamma\, s(t)$ is generated. Fig. 3(b) shows the schematics of the optical spectra after different devices for frequency-quadrupling operation.

C. Simultaneous Frequency Octupling and Phase Coding

To further improve the frequency multiplication factor, an integrated PDM-DPMZM with four RF input ports and four dc bias ports is employed. Fig. 2(b) shows the equivalent structure of the PDM-DPMZM, which consists of a PBS, two DPMZMs, and a PBC. Introducing four RF signals with different phases to the four RF ports, the output signal can be expressed as

$$\begin{cases} E_x = \cos(\omega_c t)\left[\cos\left(\beta\cos(\omega_{RF}t + \phi_1) + \dfrac{\varphi_1}{2}\right)\right. \\ \qquad\qquad \left. +\cos\left(\beta\cos(\omega_{RF}t + \phi_2) + \dfrac{\varphi_2}{2}\right)\right] \\ E_y = \cos(\omega_c t)\left[\cos\left(\beta\cos(\omega_{RF}t + \phi_3) + \dfrac{\varphi_3}{2}\right)\right. \\ \qquad\qquad \left. +\cos\left(\beta\cos(\omega_{RF}t + \phi_4) + \dfrac{\varphi_4}{2}\right)\right] \end{cases} \tag{13}$$

where φ_i (i = 1–4) represents the dc bias introduced phase in each sub-MZMs. Let $\varphi_1 = \varphi_2 = \varphi_3 = \varphi_4 = 0$ and expand (13) with Bessel functions with the exponential form

$$\begin{cases} E_x = \exp(j\omega_c t)\left\{J_0(\beta) + 2\sum_{m=1}^{\infty}(-1)^m J_{2m}(\beta)\right. \\ \qquad \times\exp[j2m(\omega_{RF}t + \phi_1)] + J_0(\beta) \\ \qquad \left. +2\sum_{m=1}^{\infty}(-1)^m J_{2m}(\beta)\exp[j2m(\omega_{RF}t + \phi_2)]\right\} \\ E_y = \exp(j\omega_c t)\left\{J_0(\beta_3) + 2\sum_{m=1}^{\infty}(-1)^m J_{2m}(\beta)\right. \\ \qquad \times\exp[j2m(\omega_{RF}t + \phi_3)] \\ \qquad J_0(\beta) + 2\sum_{m=1}^{\infty}(-1)^m J_{2m}(\beta) \\ \qquad \left. \times\exp[j2m(\omega_{RF}t + \phi_4)]\right\}. \end{cases} \tag{14}$$

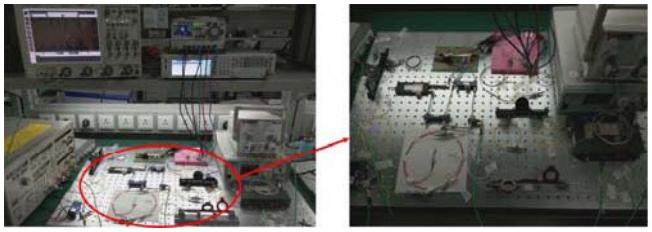

Fig. 4. Photographs of one of the experimental setups.

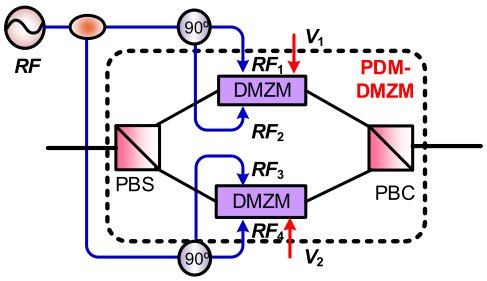

Fig. 5. Configuration of the PDM-DMZM for frequency doubling.

Setting the phases of the RF signal to let $\phi_1 = 0$, $\phi_2 = \pi/2$, $\phi_3 = \pi/8$, and $\phi_4 = 5\pi/8$, and removing the optical carrier with the wavelength fixed FBG, only sidebands with orders of $4m$ are left at the output of the orthogonally polarized CS-DSB generator

$$\begin{cases} E_x = \exp(j\omega_c t)\left[4\sum_{m=-\infty}^{\infty} J_{4m}(\beta_3)\exp(j4m\omega_{RF}t)\right] \\ E_y = \exp(j\omega_c t)\left\{4\sum_{m=-\infty}^{\infty} J_{4m}(\beta_3)\exp\left[j4m\left(\omega_{RF}t+\frac{\pi}{2}\right)\right]\right\}. \end{cases} \tag{15}$$

Due to the fact that the phase modulation index is generally smaller than 2π, the Bessel function $J_{4m}(\beta)$ for $m \geq 2$ is much smaller than $J_4(\beta)$. Therefore, higher order sidebands (>4) are neglected. With a PC followed to rotate the signal by 45° and introduce a phase difference of 90°, which is similar to the operation in the frequency-quadrupled phase-coded signal generation, we have

$$\begin{bmatrix} E_{x'} \\ E_{y'} \end{bmatrix} \propto \begin{bmatrix} \exp(j\omega_c t)\left[2J_{-4}(\beta)\exp\left(j\frac{\pi}{2} - j4\omega_{RF}t\right)\right] \\ \exp(j\omega_c t)\left[2J_4(\beta)\exp(j4\omega_{RF}t)\right] \end{bmatrix}. \tag{16}$$

As can be seen from (16), an orthogonally polarized CS-DSB signal with ±fourth-order sidebands is generated. Applying it into the microwave photonic phase coder, a phase-coded signal is generated, given by

$$I_{AC}(t) \propto J_{-4}(\beta)J_4(\beta)\cos\left(8\omega_{RF}t - \frac{\pi}{2} - 2\gamma s(t)\right). \tag{17}$$

Therefore, a frequency-octupled and phase-coded signal can be obtained. Fig. 3(c) depicts the schematics of the optical spectra under this condition.

III. Experiments and Results

To validate the proposed approaches in Fig. 1, experiments are performed. Fig. 4 shows the photos of one of the experimental setups. An optical carrier with a wavelength of 1550.998 nm is emitted from a TLS (Agilent, N7714A) and launched to a PDM-DMZM (Fujitsu, Inc., FTM7980EDA) or a PDM-DPMZM (Fujitsu, Inc., FTM7977HQA). The power of the optical wavelength at the output of TLS is 16 dBm. The 3-dB bandwidths of the PDM-DMZM and PDM-DPMZM are 31.4 and 23 GHz, respectively. The electrical driving signals are obtained by splitting the RF source (Agilent, 8257D) with a power distribution network. The power distribution network consists of several electrical power dividers (2–26.5 GHz), 90° hybrids (Krytar 3017360K, 1.7–36 GHz), phase shifters (1.8–26.5 GHz), and/or electrical attenuators, which are employed to adjust the phase and power of each driving RF signal. By carefully adjusting the phases of the driving RF signals, the orthogonally polarized double-sideband modulated signal can be generated. Then, an FBG centered at 1550.98 nm is connected to suppress the optical carrier. The bandwidth of the FBG is about 10 GHz. Since the FBG is temperature sensitive, a thermostat is used. After optical carrier suppressing, orthogonally polarized ±first-order sidebands, ±second-order sidebands, or ±fourth-order sidebands are generated, which are then directed into a 40-GHz PolM (Versawave, Inc.). The driving signal, i.e., the electrical coding signal, is generated by a pulse pattern generator (Anritsu MP1763C, 12.5 Gbits/s). PCs that contain three wave plates are employed to tune the state of the polarization of the optical signals. A 30-GHz PD with a responsivity of 0.85A/W is employed to perform optical to electrical conversion. The half-wave voltages of the PDM-DMZM, PDM-DPMZM, and PolM are all around 3.5 V. An optical spectrum analyzer (OSA, AQ6370C) and a 32-GHz real-time oscilloscope (Agilent, DSO-X 92504A) are employed to monitor the optical spectra and electrical waveforms, respectively.

A. Simultaneous Frequency Doubling and Phase Coding

To generate phase-coded signals with a doubled frequency, the PDM-DMZM is employed. To meet the required phase settings of the input RF signal to the PDM-DMZM, i.e., $\phi_1 = 0$, $\phi_2 = \pi/2$, $\phi_3 = 0$, and $\phi_4 = \pi/2$, the RF signal is first directed to a power divider, and further split into four paths with two electrical 90° hybrids, as shown in Fig. 5. DC biases of the PDM-DMZM are also adjusted to let $\varphi_1 = \pi/2$ and $\varphi_2 = -\pi/2$.

The optical spectrum measured at the output of the FBG is shown in Fig. 6. The frequency applied to the PDM-DMZM is 10 GHz. From Fig. 6, we can see that two main sidebands separated by 20 GHz are observed (solid line). To confirm the polarization orthogonality of the two sidebands, a PBS is connected. The two outputs of the PBS are shown as the dashed and dashed–dotted lines in Fig. 6. When one wavelength is selected, the other one is more than 35.9 dB lower, indicating that the two wavelengths are indeed orthogonally polarized.

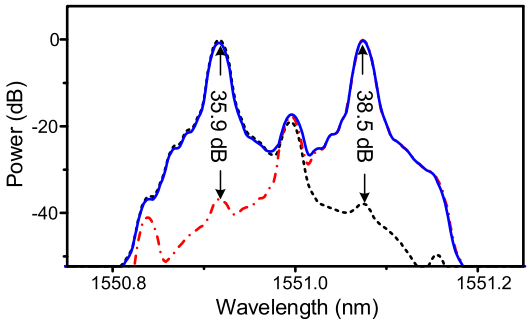

Fig. 6. Optical spectrum at the output of the notch filter (solid line) for frequency doubling, and the optical spectra at the two outputs of the PBS when a polarizer is connected to select one wavelength (dashed and dashed–dotted lines).

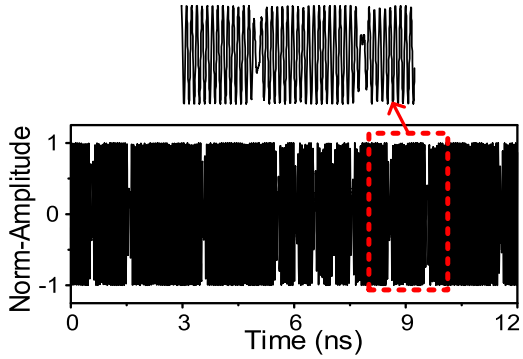

Fig. 7. Measured waveform of the generated 16-bit frequency-doubled phase-coded signal.

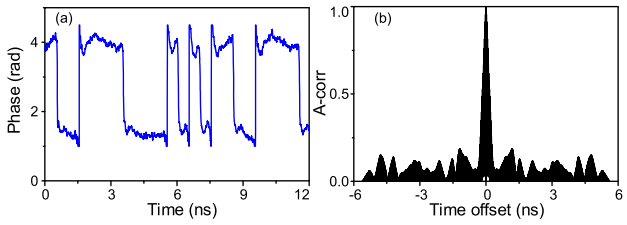

Fig. 8. (a) Phase and (b) calculated autocorrelation function of the 16-bit frequency-doubled phase-coded signal.

The two orthogonally polarized wavelengths then experience complementary phase modulations in the PolM, which is driven by a 2-Gbit/s "1111 0000 1010 1100" electrical coding signal. The waveform output from the microwave photonic phase coder is shown in Fig. 7. The central frequency is 20 GHz, i.e., double of the driving frequency 10GHz, and the phase hopping is clearly observed, especially in the zoomed-in view of the waveform. To investigate the performance of the generated frequency-doubled and phase-coded signal, its phase is recovered by Hilbert transformation, as illustrated in Fig. 8(a). A 2.7-rad phase difference between "0" and "1" is observed. The autocorrelation function of the signal is also calculated to evaluate its pulse compression capability. The full-width at half-maximum (FWHM) is calculated to be about 0.556 ns as can be seen from Fig. 8(b). The pulse compression ratio and the peak-to-sideband suppression ratio are calculated to be about 14.4 and 7.27 dB, respectively.

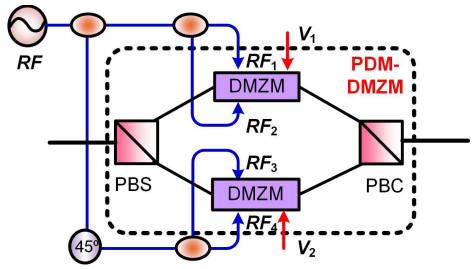

Fig. 9. Configuration of the PDM-DMZM for frequency quadrupling.

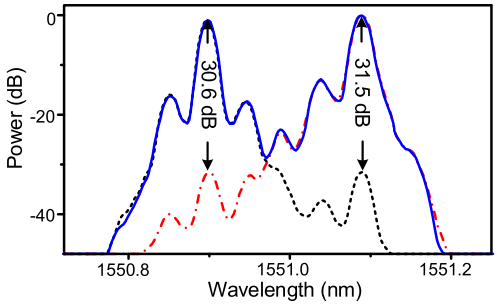

Fig. 10. Optical output of the notch filter (solid line) for frequency quadrupling, and two outputs when a PBS is connected to select the two orthogonally polarized sidebands (dashed and dashed–dotted lines).

B. Simultaneous Frequency Quadrupling and Phase Coding

The configuration of the PDM-DMZM for frequency quadrupling is shown in Fig. 9. To meet the phase settings, i.e., $\phi_1 = \phi_2 = 0$ and $\phi_3 = \phi_4 = \pi/4$, the RF source signal is first directed into a two-port power divider, and one output is phase shifted by 45° via a phase shifter. After that, the outputs are further split into four paths with other two electrical power dividers. DC biases of the PDM-DMZM are also adjusted to let $\varphi_1 = \varphi_2 = 0$.

The output of the optical orthogonally polarized CS-DSB generator is shown in Fig. 10. The electrical RF frequency is 6 GHz. The solid line is measured directly at the output of the FBG, while the dashed and dashed–dotted lines are measured when a polarizer is connected to select one of the two sidebands. The two main sidebands in the solid line are separated by 24 GHz (±second-order sidebands), and when one sideband is selected by the polarizer, the other one is suppressed by 30 dB, showing a good polarization orthogonality between the two main sidebands. The relatively low sideband suppression ratio is mainly resulting from the amplitude unbalance of the RF signals introduced to the PDM-DMZM, which could be improved if the power dividing network in Fig. 9 is carefully designed.

The experimental results for frequency-quadrupling and phase-coding operation setup are shown in Fig. 11 when a 2.4-Gbit/s "1110 0000 1100 1010" is employed to drive the PolM. Obvious phase jumps are observed from Fig. 11(a) and (b). The phase difference between "0" and "1" is observed to be about 3.14 rad. Fig. 11(c) shows the calculated autocorrelation function of the signal, whose FWHM is about 0.43 ns. The pulse compression ratio and the peak-to-sideband suppression ratio are calculated to be about 15.5 and 7.28 dB, respectively.

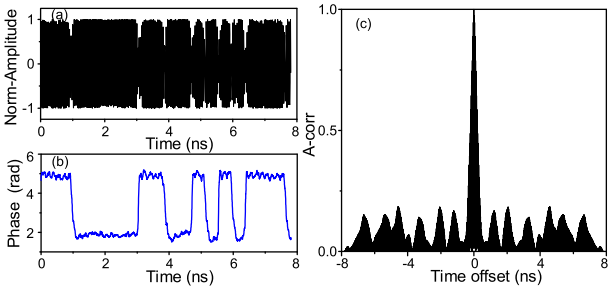

Fig. 11. Experimental results of the generated 16-bit frequency-quadrupled phase-coded signal. (a) Measured waveform. (b) Recovered phase. (c) Calculated autocorrelation function.

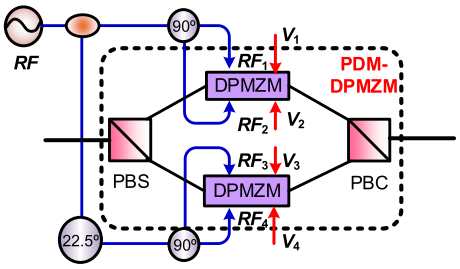

Fig. 12. Configuration of the PDM-DPMZM for frequency octupling.

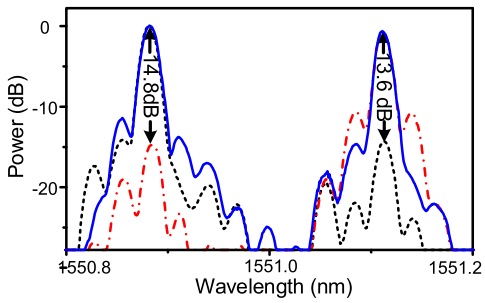

Fig. 13. Optical spectrum at the output of the notch filter (solid line) for frequency octupling, and optical outputs when a PBS is connected to select the two orthogonally polarized sidebands (dashed and dashed–dotted lines).

C. Simultaneous Frequency Octupling and Phase Coding

To simultaneously perform frequency octupling and phase coding, the PDM-DMZM is replaced by the PDM-DPMZM. To meet the phase settings of the driving RF signal required for frequency-octupled phase-coded signal generation, i.e., $\phi_1 = 0$, $\phi_2 = \pi/2$, $\phi_3 = \pi/8$, and $\phi_4 = 5\pi/8$, an electrical power divider, a phase shifter, and two 90° hybrid are employed. Fig. 12 shows the configuration of the power distribution network and the PDM-DPMZM. The RF source signal is first directed to a two-port power divider. One path is phase shifted by 22.5° via adjusting the electrical phase shifter. The two paths are then further split into four paths via two 90° hybrids. DC biases of the PDM-DPMZM are also adjusted to let $\varphi_1 = \varphi_2 = \varphi_3 = \varphi_4 = 0$.

The optical spectrum measured at the output of the FBG is shown in Fig. 13. Two large ±fourth-order sidebands are observed. Again, to examine the polarization orthogonality of the ±fourth-order sidebands, a PBS is connected to the FBG. The dashed and dashed–dotted lines in Fig. 13 show the two outputs of the PBS. In this case, the polarization extinction ratios are less than 15 dB. The poor polarization extinction ratios are mainly resulted from the unideal response of the 90° hybrid, the unideal setting of the phase shifter, and the unbalanced amplitudes of the RF signals, which also lead to the generation of many unwanted sidebands. With a 2.8-Gbit/s 16-bit sequence "1111 0000 1100 1010" applied to the PolM, a 28-GHz phase-coded signal is generated, which is eight times of the driving frequency (3.5 GHz). Since the unwanted sidebands would generate many undesirable frequency components after photodetection, an electrical filter was followed in the experiment to remove these components. Fig. 14 shows the experimental results. As can be seen, the pattern of the recovered phase agrees well with the electrical coding sequence, the phase difference between "0" and "1" is about 2.7 rad, and the FWHM of the autocorrelated pulse is about 0.33 ns. The pulse compression ratio and the peak-to-sideband suppression ratio are calculated to be about 17.3 and 6.9 dB, respectively.

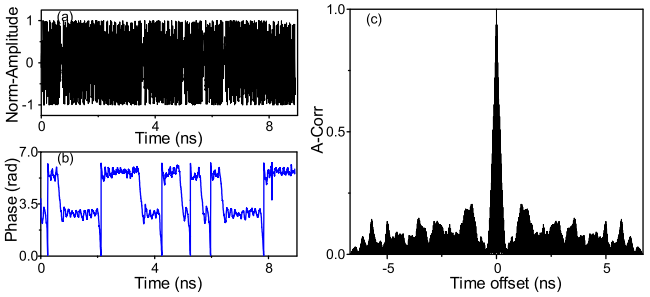

Fig. 14. Generated 16-bit frequency-octupled phase-coded signal. (a) Measured waveform. (b) Recovered phase. (c) Autocorrelation function.

IV. Discussion

A. Frequency Range of the Generated Signal

Thanks to the frequency multiplication operation, the proposed phase-coded signal generator can be operated in a large frequency range. Supposing that the frequency operation ranges of the devices employed in this scheme are $[f_{\text{MI-d}}, f_{\text{MA-d}}]$ for the power dividers, $[f_{\text{MI-ps}}, f_{\text{MA-ps}}]$ for the phase shifters, $[f_{\text{MI-h}}, f_{\text{MA-h}}]$ for the 90° hybrids, $[f_{\text{MI-m}}, f_{\text{MA-m}}]$ for the modulators, and $[f_{\text{MI-PD}}, f_{\text{MA-PD}}]$ for the PD, and the bandwidth of the FBG is B_{FBG}, the lower and upper frequency bounds of the system f_{MI} and f_{MA} should be

$$\begin{aligned} f_{\text{MI}} &= \min\{\max\{N \cdot \max\{f_{\text{MI-d}}, f_{\text{MI-ps}}, f_{\text{MI-m}}, f_{\text{MI-h}}\}, B_{\text{FBG}}\}, \\ &\qquad f_{\text{MA-PD}}\} \\ f_{\text{MA}} &= \min\{N \cdot \min\{f_{\text{MA-d}}, f_{\text{MA-ps}}, f_{\text{MA-m}}, f_{\text{MA-h}}\}, f_{\text{MA-PD}}\} \end{aligned} \tag{18}$$

where N is the frequency multiplication factor, max{} chooses the maximum value from the braces, and min{} chooses the minimum one. With the experimental setup in this paper for frequency-doubled phase-coded signal generation, $f_{\text{MI-d}} = 2$ GHz, $f_{\text{MA-d}} = 26.5$ GHz, $f_{\text{MI-h}} = 1.7$ GHz, $f_{\text{MA-h}} = 36$ GHz, $f_{\text{MI-m}} =\sim 0$ GHz, $f_{\text{MA-m}} = 31.4$ GHz, $f_{\text{MI-ps}} = 1.8$ GHz, $f_{\text{MA-ps}} = 26.5$ GHz, $f_{\text{MA-PD}} = 30$ GHz, and $B_{\text{FBG}} = 10$ GHz. f_{MI} is calculated to be 10 GHz, which is restricted by B_{FBG}, and f_{MA} is calculated to be 30 GHz,

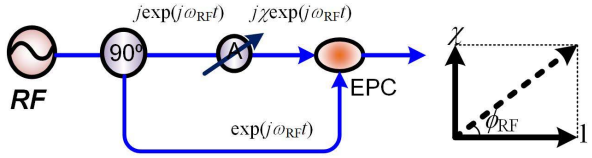

Fig. 15. Schematic for broadband phase shifts. EPC: electrical power combiner.

which is constrained by $f_{\text{MA-PD}}$. Similarly, we can obtain that f_{MI} and f_{MA} for frequency quadrupling situation are 10 and 30 GHz, respectively, which are also restricted by B_{FBG} in the lower bound and $f_{\text{MA-PD}}$ in the upper bound. For the frequency-octupled phase-coded signal generation, f_{MI} and f_{MA} are calculated to be 16 and 30 GHz, respectively, which are limited by the electrical power divider in the lower bound and the 3-dB bandwidth of the PD in the upper bound.

It should be noted that the 3-dB bandwidth of the commercial available FBG can be tens of megahertz [27], so the lowest frequencies for frequency-doubling, frequency-quadrupling, and frequency-octupling and phase-coding systems can be 4, 8, and 16 GHz, respectively, limited by the lowest operational frequency of the power divider. In addition, the bandwidth of the PD reported in the literature can be as high as 500 GHz [28]. If it is employed, the maximum operational frequencies of the frequency-doubled, frequency-quadrupled, and frequency-octupled phase-coded signals' generator can be extended to 53, 106, and 184 GHz, respectively, restricted by $f_{\text{MA-d}}$ and $f_{\text{MA-m}}$.

In addition, if electrical devices and optical modulator with higher bandwidth are employed, generation of terahertz phase-coded signal is possible.

B. Broadband Phase Shift

In the phase-coded signal generator, RF signals should undergo 0, $\pi/8$, $\pi/4$, or $\pi/2$ phase shift. If electrical phase shifters are utilized, the frequency tunability will be significantly affected because the phase shifters are frequency dependent. To solve this problem, broadband phase shifts can be generated based on vector sum of two orthogonal RF signals with variable amplitudes. Fig. 15 shows one of such schemes to produce the broadband phase shifts based on a broadband 90° hybrid, an attenuator, and a power divider.

Suppose that the expressions of the signals at the two outputs of the 90° hybrid are $\exp(j\omega_{\text{RF}}t)$ and $j\exp(j\omega_{\text{RF}}t)$. When an electrical attenuator is connected to the orthogonal output of the 90° hybrid, the signal becomes $j\chi\exp(j\omega_{\text{RF}}t)$, where χ is the attenuation coefficient. With a power combiner to combine the two signals, we obtain an RF signal in the form of

$$\begin{aligned} E_{\text{RF}}(t) &= (1+j\chi)\exp(j\omega_{\text{RF}}t) \\ &= \sqrt{1+\chi^2}\exp(j\omega_{\text{RF}}t + j\phi_{\text{RF}}). \end{aligned} \tag{19}$$

Therefore, an electrical signal with its phase shifted by ϕ_{RF} is obtained, where $\phi_{\text{RF}} = \arccos(1/(1+\chi^2)^{0.5})$. Because the bandwidth of the 90° hybrid, the attenuator, and the power combiner can be very large, ϕ_{RF} can be almost frequency independent.

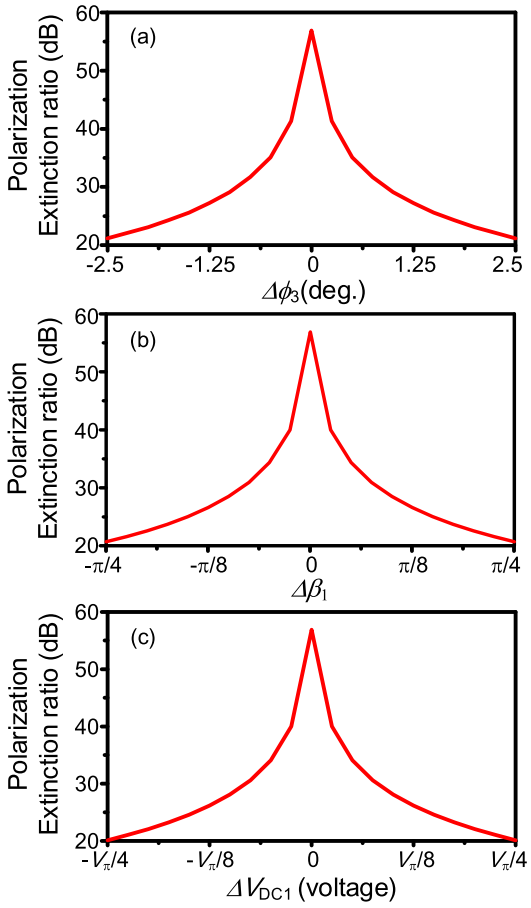

Fig. 16. Polarization extinction ratio as a function of (a) $\Delta\phi_3$, (b) $\Delta\beta_1$, and (c) ΔV_{DC1}.

C. Polarization Orthogonality of the Two Sidebands and Its Impact

The proposed system highly desires that the two sidebands introduced to the PolM-based microwave photonic phase coder are orthogonally polarized. To generate such sidebands, the phases of the RF signals to the four RF input ports should be controlled to achieve the required values of ϕ_1–ϕ_4, and the amplitudes should be adjusted to let the modulation indices of the four branches in the modulator identical. In addition, the bias voltages of the modulator should be controlled to obtain the required values of φ_1–φ_4. However, it is very hard to achieve these conditions simultaneously, thanks to the unideal response of the phase shifters, the unideal design of the power dividing network, and the bias drifts of the modulator. To evaluate the influence of these nonidealities on the polarization orthogonality of the two sidebands, a numerical simulation of the frequency-octupling and phase-coding operation is carried out based on OptiSystem 12.0 (Optiwave, Inc.). A parameter named polarization extinction ratio is also defined, which is the power ratio of one sideband to the other sideband along a polarization direction that the former achieves maximum power.

Fig. 16 shows the simulated results when the phase of one RF signal (ϕ_3), the modulation index of one sub-MZM in the PDM-DPMZM (β_1), or one dc bias of the modulator (V_{DC1}) deviates from its ideal value. From the results, we can conclude

that the polarization extinction ratio monotonically decreases when the deviation of the three parameters increases. To maintain a 20-dB polarization extinction ratio, the variation range is $\pm 2.5^\circ$ for ϕ_3, $\pm\pi/4$ for β_1, and $\pm V_\pi/4$ for V_{DC1}, indicating that all the parameters should be carefully controlled. In practice, two or more parameters may drift simultaneously. In that case, the polarization extinction ratio will be further degraded. For example, when the aforementioned three parameters ϕ_3, β_1, and V_{dc1} drift by 2.5°, $\pi/4$, and $V_\pi/4$ at the same time, the polarization extinction ratio will be decreased to 15 dB, and if all the phases, the modulation indices, and the dc biases drift simultaneously, the polarization extinction ratio will be lower than 10 dB.

The unideal polarization orthogonality of the two sidebands would result in performance degradation. Take the frequency-octupled phase-coded signal generation as an example again; if the polarization extinction ratio is too low, the output of the orthogonally polarized CS-DSB generator can be rewritten as

$$\begin{bmatrix} E_{x'} \\ E_{y'} \end{bmatrix} \propto \exp\ (j\omega_c t) \begin{bmatrix} \exp(-j4\omega_{\mathrm{RF}}t) + \alpha^{-1}\exp(j4\omega_{\mathrm{RF}}t) \\ \alpha^{-1}\exp(-j4\omega_{\mathrm{RF}}t) + \exp(j4\omega_{\mathrm{RF}}t) \end{bmatrix} \tag{20}$$

where α is the polarization extinction ratio in linear scale and $\alpha \geq 1$. Introducing the signal to the PolM for complementary phase modulations, and beating them at the PD

$$\begin{aligned} I(t) \propto\ & 4\alpha^{-1}\cos(8\omega_{RF}t) \\ & + 2\alpha^{-2}\cos(8\omega_{RF}t + 2\gamma s(t)) \\ & + 2\cos(8\omega_{RF}t - 2\gamma s(t)) \end{aligned} \tag{21}$$

when $\alpha = \infty$, which refers to the ideal polarization orthogonality of the two sidebands, only the last term is left, and an ideal frequency-octupled phase-coded signal is obtained. When $\alpha = 1$, which represents that the two sidebands are in the same polarization state, (20) becomes

$$I(t) \propto (4 + 4\cos(2\gamma s(t)))\cos(8\omega_{RF}t). \tag{22}$$

Therefore, a purely intensity-coded signal is obtained. When α is other value, the generated signal will contain both the phase-coded and the intensity-coded frequency-octupled signals. As a result, the performance of the generated signal is degraded. The simulated results and the autocorrelation functions with different values of α are shown in Fig. 17. From Fig. 17, we can see that, for the $\alpha = \infty$ case, the amplitude of the generated signal maintains unchanged and the calculated autocorrelation function has a good pulse compression capability. When α becomes smaller, the amplitude of the generated signal is partly intensity modulated, and the compressed pulse obtained by autocorrelation is broadened. For the worst case ($\alpha = 1$), only intensity modulated signal is obtained and the pulse compression capability is lost. It should be noted that different phase modulations are presented in Fig. 17(c) and (e) although their profiles look similar. The two insets of Fig. 17 show the zoomed-in views of the two waveforms at the jump point. As can be seen, there is no phase jump in Fig. 17(e) although the amplitude is varied.

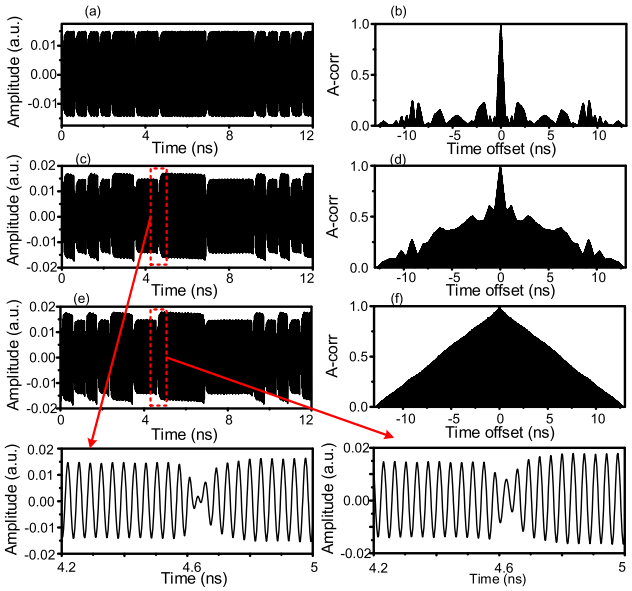

Fig. 17. Waveforms and autocorrelation functions of the simulated frequency-octupled phase-coded signals when (a) and (b) $\alpha = \infty$, (c) and (d) $\alpha = 2$, and (e) and (f) $\alpha = 1$.

V. Conclusion

A novel frequency-multiplied phase-coded signal generator based on an integrated PDM-DMZM or PDM-DPMZM was proposed and experimentally demonstrated. The frequency multiplication operation makes the generator capable to operate within a frequency range far more beyond the working frequency range of the devices used in the scheme. Theoretical analysis of the simultaneous frequency multiplying and phase coding was performed. Experiments to study the performance of the system were carried out. Phase-coded signals with a frequency multiplication factor of two, four, or eight were generated. The recovered coding signals and the pulse compression capabilities were evaluated. The performance of the generated signals related to the polarization extinction ratio was also discussed. The proposed method features compact configuration and large operational frequency range, which can be employed in radar systems and terahertz signal generation systems.

References

[1] M. I. Skolnik, *Introduction to Radar Systems*. New York, NY, USA: McGraw-Hill, 1962.

[2] J. Yao, "Microwave photonics," *J. Lightw. Technol.*, vol. 27, no. 3, pp. 314–335, Feb. 1, 2009.

[3] S. L. Pan, D. Zhu, and F. Z. Zhang, "Microwave photonics for modern radar systems," *Trans. Nanjing Univ. Aeronautics Astron.*, vol. 31, no. 3, pp. 219–240, Jun. 2014.

[4] L. Gao, X. Chen, and J. Yao, "Photonic generation of a phase-coded microwave waveform with ultrawide frequency tunable range," *IEEE Photon. Technol. Lett.*, vol. 25, no. 10, pp. 899–902, May 2013.

[5] W. Li, L. X. Wang, M. Li, and N. H. Zhu, "Photonic generation of widely tunable and background-free binary phase-coded radio-frequency pulses," *Opt. Lett.*, vol. 38, no. 17, pp. 3441–3444, Sep. 2013.

[6] W. Li, L. X. Wang, M. Li, H. Wang, and N. H. Zhu, "Photonic generation of binary phase-coded microwave signals with large frequency tunability using a dual-parallel Mach–Zehnder modulator," *IEEE Photon. J.*, vol. 5, no. 4, Aug. 2013, Art. no. 5501507.

[7] Z. Tang, T. Zhang, F. Zhang, and S. Pan, "Photonic generation of a phase-coded microwave signal based on a single dual-drive Mach–Zehnder modulator," *Opt. Lett.*, vol. 38, no. 24, pp. 5365–5368, Dec. 2013.

[8] W. Li, W. T. Wang, W. H. Sun, and N. H. Zhu, "All-optical generation of binary phase-coded microwave signal based on cross-polarization modulation in a highly nonlinear fiber," *Opt. Lett.*, vol. 39, no. 6, pp. 1561–1564, Mar. 2014.
[9] J. Chou, Y. Han, and B. Jalali, "Adaptive RF-photonic arbitrary waveform generator," *IEEE Photon. Technol. Lett.*, vol. 15, no. 4, pp. 581–583, Apr. 2003.
[10] J. Ye *et al.*, "Photonic generation of microwave phase-coded signals based on frequency-to-time conversion," *IEEE Photon. Technol. Lett.*, vol. 24, no. 17, pp. 1527–1529, Sep. 2012.
[11] C. Wang and J. Yao, "Phase-coded millimeter-wave waveform generation using a spatially discrete chirped fiber Bragg grating," *IEEE Photon. Technol. Lett.*, vol. 24, no. 17, pp. 1493–1495, Sep. 2012.
[12] P. Ghelfi, F. Scotti, F. Laghezza, and A. Bogoni, "Photonic generation of phase-modulated RF signals for pulse compression techniques in coherent radars," *J. Lightw. Technol.*, vol. 30, no. 11, pp. 1638–1644, Jun. 2012.
[13] Z. Li, W. Li, H. Chi, X. Zhang, and J. Yao, "Photonic generation of phase-coded microwave signal with large frequency tunability," *IEEE Photon. Technol. Lett.*, vol. 23, no. 11, pp. 712–714, Jun. 2011.
[14] H.-Y. Jiang, L.-S. Yan, J. Ye, W. Pan, B. Luo, and X. Zou, "Photonic generation of phase-coded microwave signals with tunable carrier frequency," *Opt. Lett.*, vol. 38, no. 8, pp. 1361–1363, Apr. 2013.
[15] W. Li, W. T. Wang, W. H. Sun, L. X. Wang, and N. H. Zhu, "Photonic generation of arbitrarily phase-modulated microwave signals based on a single DDMZM," *Opt. Exp.*, vol. 22, no. 7, pp. 7446–7457, Apr. 2014.
[16] W. Li, F. Kong, and J. Yao, "Arbitrary microwave waveform generation based on a tunable optoelectronic oscillator," *J. Lightw. Technol.*, vol. 31, no. 23, pp. 3780–3786, Dec. 1, 2013.
[17] H. Chi and J. Yao, "Photonic generation of phase-coded millimeter-wave signal using a polarization modulator," *IEEE Microw. Wireless Compon. Lett.*, vol. 18, no. 5, pp. 371–373, May 2008.
[18] Z. Li, M. Li, H. Chi, X. Zhang, and J. Yao, "Photonic generation of phase-coded millimeter-wave signal with large frequency tunability using a polarization-maintaining fiber Bragg grating," *IEEE Microw. Wireless Compon. Lett.*, vol. 21, no. 12, pp. 694–696, Dec. 2011.
[19] W. Li, N. H. Zhu, and L. X. Wang, "Perfectly orthogonal optical single-sideband signal generation based on stimulated Brillouin scattering," *IEEE Photon. Technol. Lett.*, vol. 24, no. 9, pp. 751–753, May 1, 2012.
[20] Y. Zhang and S. Pan, "Generation of phase-coded microwave signals using a polarization-modulator-based photonic microwave phase shifter," *Opt. Lett.*, vol. 38, no. 5, pp. 766–768, Mar. 2013.
[21] S. Liu, D. Zhu, Z. Wei, and S. Pan, "Photonic generation of widely tunable phase-coded microwave signals based on a dual-parallel polarization modulator," *Opt. Lett.*, vol. 39, no. 13, pp. 3958–3961, Jul. 2014.
[22] Y. Zhang, F. Zhang, and S. Pan, "Frequency-doubled and phase-coded RF signal generation based on orthogonally polarized carrier-suppressed double sideband modulation," in *Proc. Asia Commun. Photon. Conf. (ACP)*, 2014, paper AF3A-2.
[23] X. Li, S. Zhao, Y. Zhang, Z. Zhu, and S. Pan, "Generation of a frequency-quadrupled phase-coded signal with large tunability," *IEEE Photon. Technol. Lett.*, vol. 28, no. 18, pp. 1980–1983, Sep. 2016.
[24] S. Pan and Y. Zhang, "Tunable and wideband microwave photonic phase shifter based on a single-sideband polarization modulator and a polarizer," *Opt. Lett.*, vol. 37, no. 21, pp. 4483–4485, Nov. 2012.
[25] Y. Zhang, F. Zhang, and S. Pan, "Optical single sideband polarization modulation for radio-over-fiber system and microwave photonic signal processing," *Photon. Res.*, vol. 2, no. 4, pp. B80–B85, Aug. 2014.
[26] S. Pan, P. Zhou, Z. Tang, Y. Zhang, F. Zhang, and D. Zhu, "Optoelectronic oscillator based on polarization modulation," *Fiber Integr. Opt.*, vol. 34, no. 4, pp. 185–203, Oct. 2015.
[27] M. Poulin *et al.*, "Ultra-narrowband fiber Bragg gratings for laser linewidth reduction and RF filtering," *Proc. SPIE*, vol. 7579, p. 75791C, Feb. 2010.
[28] F. Xia, T. Mueller, Y. Lin, A. Valdes-Garcia, and P. Avouris, "Ultrafast graphene photodetector," *Nature Nanotechnol.*, vol. 4, no. 12, pp. 839–843, Oct. 2009.

Yamei Zhang (S'13) received the B.S. degree from the Nanjing University of Aeronautics and Astronautics, Nanjing, China, in 2012, where she is currently pursuing the Ph.D. degree at the Key Laboratory of Radar Imaging and Microwave Photonics, Ministry of Education.

Her current research interests include microwave photonic signal generation and processing.

Fangzheng Zhang received the B.S. degree from the Huazhong University of Science and Technology, Wuhan, China, in 2008, and the Ph.D. degree from the Beijing University of Posts and Telecommunications, Beijing, China, in 2013.

He is currently with the Key Laboratory of Radar Imaging and Microwave Photonics, Nanjing University of Aeronautics and Astronautics, Ministry of Education. His current research interests include microwave photonics, coherent optical communications, and all-optical signal processing.

Shilong Pan (S'06–M'09–SM'13) received the B.S. and Ph.D. degrees in electronics engineering from Tsinghua University, Beijing, China, in 2004 and 2008, respectively.

From 2008 to 2010, he was a "Vision 2010" Postdoctoral Research Fellow with the Microwave Photonics Research Laboratory, University of Ottawa, Ottawa, ON, Canada. He joined the College of Electronic and Information Engineering, Nanjing University of Aeronautics and Astronautics, Nanjing, China, in 2010, where he is currently a Full Professor and the Executive Director with the Key Laboratory of Radar Imaging and Microwave Photonics, Ministry of Education. He has authored or co-authored over 260 research papers, 140 papers in peer-reviewed journals, and 120 papers in conference proceedings. His research is focused on microwave photonics, which include the optical generation and processing of microwave signals, ultra-wideband over fiber and its applications, photonic microwave measurement, and integrated microwave photonics.

Prof. Pan is a Senior Member of the IEEE Microwave Theory and Techniques Society and the IEEE Photonics Society. He is a member of the Optical Society of America. He was the Chair of numerous international conferences and workshops, including the TPC Chair of the International Conference on Optical Communications and Networks in 2015, the TPC Chair of the High-Speed and Broadband Wireless Technologies Subcommittee of the IEEE Radio Wireless Symposium in 2013, 2014, and 2016, the TPC Chair of the Optical Fiber Sensors and Microwave Photonics Subcommittee of the OptoElectronics and Communication Conference in 2015, and the Chair of the Microwave Photonics for Broadband Measurement Workshop of the IEEE MTT-S International Microwave Symposium in 2015. He was a recipient of the OSA Outstanding Reviewer Award in 2015.